

# An Analytical Model for Predicting the Remaining Battery Capacity of Lithium-Ion Batteries

Peng Rong, *Student Member, IEEE* and Massoud Pedram, *Fellow, IEEE*

**Abstract**— Predicting the residual energy of the battery source that powers a portable electronic device is imperative in designing and applying an effective dynamic power management policy for the device. The paper starts up by showing that a 30% error in predicting the battery capacity of a Lithium-ion battery can result in up to 20% performance degradation for a dynamic voltage and frequency scaling algorithm. Next, this paper presents a closed-form analytical expression for predicting the remaining capacity of a lithium-ion battery. The proposed high-level model, which relies on online current and voltage measurements, correctly accounts for the temperature and cycle aging effects. The accuracy of the high-level model is validated by comparing it with DUALFOIL simulation results, demonstrating a maximum of 5% error between simulated and predicted data.

**Index Terms**—Remaining battery capacity, accelerated rate capacity, temperature, cycle aging and dynamic voltage scaling

## I. INTRODUCTION

THE battery service life of mobile battery-powered electronic systems is a major concern of designers of such systems. Attempts for extending the battery lifetime have traditionally focused on minimizing the power consumption of the electronic circuits powered by these batteries. These circuit-oriented techniques tend to be inadequate because they ignore important characteristics of the battery source itself e.g., the dependency of the remaining capacity of a secondary (rechargeable) battery on its current discharge rate and internal temperature, the charge recovery phenomenon, and the cycle aging effect. In the recent years, a number of researchers have begun to investigate the characteristics of battery sources and their impact on low-power circuit optimization techniques and power management strategies. A survey of battery-aware design techniques can be found in reference [1][2].

A number of researchers have reported models for predicting the battery remaining capacity or battery service life. A low-level detailed electrochemical model based on concentrated-solution theory was reported in [3]. This model is accurate and general enough to handle a wide range of lithium-ion cells, which also explains the wide-spread use of its companion simulator software. A multi-dimensional coupled thermal-electrochemical model was presented in [4].

Electrochemical models are accurate but inherently suffer from the long simulation time required in practice.

Consequently, more efficient battery models have been proposed in recent years. A macro-model for lithium-ion batteries was presented in [5], where the battery is modeled by a PSPICE circuit comprising of voltage sources and linear passive elements. Since simulation of the electrical circuit model is still time consuming, the authors of reference [6] proposed a discrete-time battery simulation model, which approximates a continuous-time circuit model by using VHDL language. Reference [7] studied the battery discharge efficiency under different loading conditions and approximated this dependency as a linear or quadratic function. In this paper, the authors also presented a discharge rate-based method to estimate the battery lifetime under a variable load. The battery discharge efficiency was used as the weighting coefficient in the lifetime estimation equation.

Reference [8] presented a stochastic battery model based on discrete Markovian process which captures battery recovery and rate capacity effects. Reference [9] proposed a high-level diffusion based analytical model. This model aims to predict the battery lifetime given the discharge profile. The authors consider the concentration evolution of the active materials in the battery during a discharge process and model it as a one-dimensional diffusion process in a finite region. In this model, a battery is considered exhausted when the active material concentration at the electrode surface drops below a preset threshold. This model is quite successful in terms of prediction accuracy, efficiency and generality. However, a prerequisite to use this model is that the load of a battery should be known exactly from the beginning of a discharge process. And this model does not take temperature dependence and cycle aging effects in account. So each time when a battery works in a different situation the model parameters needs to be reset, which may cause inconvenience in practice due to the overhead. An extensive review of battery models and battery aware low power techniques can be found in the [10].

The battery temperature and the cycle life of a secondary battery have a large impact on the battery lifetime after a full charging step. As temperature increases, the full discharge capacity of a secondary battery tends to increase. Unfortunately, higher temperature also results in much lower *cycle-life* for the battery (the cycle-life denotes the number of full charge/discharge cycles that a secondary battery can go thru before its output voltage drops below an acceptable threshold even after a full charging cycle.) The battery cycle aging effect denotes the phenomenon by which the full deliverable capacity of a rechargeable battery decreases as the number of battery charge/discharge cycles (which is referred to as the *cycle-age* of the battery) increases. As shown in work [11], the full deliverable capacities of commercial lithium-ion batteries shrink by 10-40% during the first 450

---

Manuscript received February 2, 2003, revised July 14, 2005 and accepted January 23, 2006. This work was funded in part by a grant from the NSF CSR-EHS program (contract # 0509564.)

P. Rong is with Department of Electrical Engineering, University of Southern California, CA 90089, USA (email: prong@usc.edu).

M. Pedram is with Department of Electrical Engineering, University of Southern California, CA 90089, USA (email: pedram@usc.edu).

charge/discharge cycles. Without knowledge about temperature and cycle life of a battery, it is therefore impossible to obtain an accurate prediction of the battery remaining capacity.

Commercially deployed battery estimation techniques can be generally classified into three categories according to their expected accuracy: load voltage technique [12], coulomb counting technique [13], and internal resistance method [14]. The load voltage technique is suitable for applications with constant load. The coulomb counting technique accumulates the dissipated coulombs from the beginning of the discharge cycle and estimates the remaining capacity based on the difference between the accumulated value and a pre-recorded full-charge capacity. This method can lose some of its accuracy under variable load condition because it ignores the non-linear discharge effect during the coulomb counting process. The internal resistance method needs to measure the frequency response of the battery to determine its battery state. Because this method normally requires extra function generators and separate testing period, this method is expensive and difficult to implement as part of the battery pack itself.

This paper presents an analytical model to predict the remaining capacity of a lithium-ion battery. The model takes the cycle-aging and temperature effects into account. This model requires small storage space, which is important since the amount of memory in the battery pack is usually limited. In addition, the proposed model relies on simple measurements of the battery output voltage and temperature, which can be easily achieved through the “smart battery” technology and corresponding interface. Starting from this analytical model, we present a method for predicting the remaining capacity of the battery under variable load conditions. This method makes use of information about the battery’s discharge history in the current charge/discharge cycle through a coulomb counting mechanism.

The paper is organized as follows: In Section 2, a motivating application is provided to demonstrate the importance of correctly predicting battery remaining capacity. In Section 3, the basic electrochemical background of cells is introduced. The model which is first promoted in this paper and is used to estimate the remaining battery capacity is described in Section 4. Model validation results are presented in Section 5. Techniques for online prediction of the remaining battery capacity are presented in Section 6. Finally, conclusions are given in Section 7.

## II. MOTIVATING APPLICATION

Dynamic voltage and frequency scaling (DVFS) is a highly effective method to reduce energy consumption in real-time applications. Reducing the supply voltage can significantly reduce the energy dissipation of a VLSI circuit but can also slow down the circuit. The energy dissipation of a running CMOS VLSI circuit is given by the well-known equation:

$$E = C_{switched} V^2 f_{clk} T \quad (2-1)$$

where  $V$  is the supply voltage level,  $C_{switched}$  is the switched capacitance per clock cycle,  $f_{clk}$  is the frequency of the processor,  $T$  is the total execution time.

*Utility*, which was initially motivated by Shenker [15] to use in modeling of a user’s relative satisfaction for a real-time stream which is encoded at varying levels of fidelity, has been applied to the design of a wide range of systems running various types of applications [15][16][17]. A utility function maps the service delivered by a system into a real value which measures the performance of the application in terms of user perception. In the following, we will consider a scenario of utility-based DVFS for battery-power embedded systems. Martin [18] analyzed the power-performance trade-off for CPU speed-setting for mobile computing, where the number of computations performed per complete battery discharge is used as the optimization objective. This work takes the battery rate-capacity effect into consideration.

Consider a partially-discharged secondary battery as the power source of an embedded system. Let’s assume the system has to complete a series of real-time tasks during the remaining battery lifetime. The *utility rate* is assumed to be a function of  $f_{clk}$ , i.e.,  $u = u(f_{clk})$ . Total utility,  $U$ , is calculated as

$$U(V, f_{clk}) = \int_0^{T_{rem}(V, f_{clk})} u(f_{clk}) dt \quad (2-2)$$

where  $T_{rem}(V, f_{clk})$  refers to the remaining battery lifetime given that the circuit is running at frequency  $f_{clk}$  with supply voltage  $V$  (notice that  $V$  is the output of the DC-DC-converter.) Thus the problem of utility-based DVFS is formulated as

$$\max_{V, f_{clk}} U(V, f_{clk}), \quad (2-3)$$

where

$$f_{clk} = mV + q, \quad (2-4)$$

where  $m$  and  $q$  are the regression coefficients of the best linear fit between the clock frequency and the supply voltage in the performance range of interest. To make this optimization problem analytically solvable, let’s assume that  $f_{clk}$  remains constant for the remaining time. Now we have

$$U(V, f_{clk}) = u(f_{clk}) T_{rem}(V, f_{clk}). \quad (2-5)$$

Consider that at the beginning of this operation, the remaining ideal battery charge is  $E_{init}$ . Let  $i_B$  denote the current drawn from the battery while  $V_B$  denotes the battery output voltage (notice that  $V_B$  is the input to the DC-DC converter.)

We thus have:  $i_B = \frac{C_{switched} V^2 f_{clk}}{\eta V_B}$ , where  $0 < \eta \leq 1$  is a constant,

capturing the DC-DC converter efficiency factor. If we ignore the battery characteristics, as has been done in the past, the utility function may be expressed as

$$U(V, f_{clk}) = u(f_{clk}) \frac{E_{init}}{i_B V_B} = \frac{\eta E_{init} u(f_{clk})}{C_{switched} V^2 f_{clk}}. \quad (2-6)$$

This formulation does not, for example, take the battery rate-capacity effect into account. To overcome this drawback, we incorporate a function  $\beta(i_B)$  into the formulation (2-6), which captures the effect that the deliverable battery capacity decreases as the discharge rate increases. As discussed by Wu and Pedram [7],  $\beta(i_B)$  can be modeled by a linear up to a quadratic function of  $i_B$ . Now, the above equation can be rewritten as

$$U(V, f_{clk}) = u(f_{clk}) \frac{E_{init}}{i_B V_B \beta'(i_B)} = \frac{\eta E_{init} u(f_{clk})}{C_{switched} V^2 f_{clk} \beta'(i_B)} \quad (2-7)$$

However, this equation still makes the assumption that the battery discharge characteristics are unchanged throughout the whole discharge period, which rarely holds during discharge of a real battery employed in a real system.

To make the dependence of  $U$  on variable  $V$ , we replace  $\beta(i_B)$  with  $\beta(V)$  and  $f_{clk}$  with  $mV+q$ , resulting in

$$U(V) = \frac{\eta E_{init} u(mV+q)}{C_{switched} V^2 (mV+q) \beta(V)} \quad (2-8)$$

The simulation results of a Bellcore PLION cell by using DUALFOIL program [3] are presented in Figure 1. In this figure, each point is obtained in the following way. First, we discharge a fresh battery at a very low rate, i.e. 0.1C, to a certain state of the battery remaining charge, which is the x-axis value of this point. Next, this battery is discharged from the current state to exhaustion at X.C rate. The points on any continuous curve in the figure have the same X value, which is reported beside the corresponding curve. All discharges took place at 25°C. Notice that the “1C” rate denotes a rate at which a fresh battery will be discharged to exhaustion in an hour at room temperature.

From this figure, we can draw the following conclusions: (a) The Bellcore PLION cell exhibits the *standard rate-capacity phenomenon*. This can be seen, for example, by noting the degradation of the deliverable capacity of a fully-charged battery from a normalized value of 1 at a discharge rate of X=0.1C to about 0.68 at a discharge rate of X=1.33. (b) The Bellcore PLION cell also exhibits an *accelerated rate-capacity behavior* in the sense that if, for example, the battery is already half discharged, then the capacity loss for the remaining discharge process will go from a normalized value of 1 at a discharge rate of X=0.1C to about 0.52 at a discharge rate of X=1.33. In other words, the rate-capacity effect becomes more prominent at lower states of battery charge.

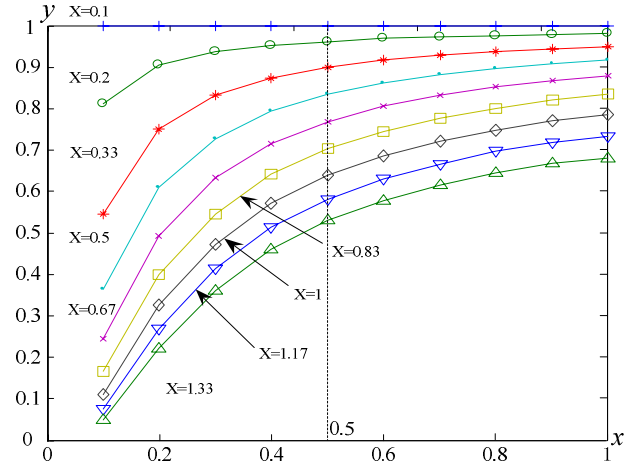


**Figure 1. Accelerated rate-capacity behavior; the x axis denotes the battery state of charge after partial discharge at a rate of 0.1C whereas the y axis denotes ratio of the remaining battery capacity at X.C discharge rate to that at 0.1C discharge rate.**

From (2-8) we can obtain the optimal value of  $V$  as

$$\frac{dU}{dV} = 0 \Rightarrow \frac{m\beta(V)}{u(mV)} \frac{du}{df_{clk}} - \frac{d\beta}{dV} = \frac{2}{V} - \frac{1}{mV+q} \quad (2-9)$$

For the conventional approach which ignores the battery characteristics (cf. equation (2-6)), the optimal  $V$  value can be obtained from (2-9) by letting  $u(mV) \equiv 1$  and  $\frac{d\beta}{dV} \equiv 0$ . These solutions are static, and therefore, unrelated to the dynamic state of charge of the battery. However, if we attempt to account for the accelerated rate-capacity behavior of lithium ion batteries, then  $\beta$  cannot be taken as constant any more. That is, we ought to make  $\beta$  a function of  $V$  and battery charge state  $s$ , i.e., we must use  $\beta(V, s)$ . Thus, the total utility is calculated as

$$U(V, f_{clk}, s) \approx \frac{u(mV)}{V^2 (mV+q) \beta(V, s)} \quad (2-10)$$

The optimal value of  $V$  is a solution of

$$\frac{m\beta(V, s)}{u(mV)} \frac{du}{df_{clk}} - \frac{\partial \beta(V, s)}{\partial V} = \frac{2}{V} - \frac{1}{mV+q} \quad (2-11)$$

To solve this optimization problem, it is important to calculate the correct value of  $\beta(V, s)$ , which in turn, as demonstrated in Figure 1, requires an accurate method to estimate the battery’s remaining capacity at different discharge rates.

To quantitatively evaluate the impact of accelerated rate-capacity behavior on the performance of the utility-based DVFS technique, let’s consider a real case: a voltage-frequency adjustable Xscale processor running a rate-adaptive real-time application, powered by a Bellcore battery whose rate-capacity behavior is shown in Figure 1. We assume this battery has a C-rate of 250mA, which is equivalent to six

Bellcore's PLION cells connected in parallel. As reported in [19], the clock frequency of the Xscale processor in GHz is related to the supply voltage in the form of equation:  $f_{clk} = 0.9629V - 0.5466$ , which is a best fit of the measuring points when  $f_{clk}$  is in the range of 0.333 to 0.667 GHz. The power consumption of the Xscale processor at clock frequency 667MHz is 1.16W, which discharges the battery at a rate of 335mA.

By assuming that the frequency-voltage level is continuously adjustable, we attempt to find out the optimal voltage level which maximizes the total utility during the remainder of the battery lifetime. In this example problem setup, we consider the following utility rate function:  $u(f_{clk}) = (3f_{clk} - 1)^\theta, \theta > 0$ , which evaluates to 1 at 666MHz and to 0 at 333MHz. Clearly, such a function means that the performance is completely satisfying at 666MHz while it is completely unacceptable at 333MHz. The particular functional form is chosen because utility-rate curves with different shapes, i.e., concave, convex and linear, may be obtained by simply adjusting the value of parameter  $\theta$ . The simulation results, when  $\theta=0.5, 1$  and  $1.5$ , are reported in the following table.

For a comparison, we consider different methods to determine the optimal voltages. The first method determines the optimal voltage based on the rate-capacity characteristic of a fully-charged battery. For these two methods, the CPU voltage is determined by solving equation (2-9). The second method determines the optimal voltage setting based on a coulomb counting mechanism, which estimates the remaining battery capacity by subtracting the delivered capacity from the nominal capacity.

In Table I these two methods are referred as MRC and MCC, respectively. In the third and final method, denoted by Mopt, the operating voltage is set to a value that maximizes the total utility based on the actual accelerated rate-capacity curves as shown in Figure 1. With this method, the CPU voltage is determined by solving equation (2-11). In this table, the "Vopt" column under each method contains the "optimal" voltage value determined by this method whereas the corresponding simulated utility values appear in column "Util". The utility values shown in this table are relative values as compared to the utility obtained with the MRC method, which is in turn normalized to 1 (not shown in the table.)

From this table, it is observed that an accurate estimation of battery remaining capacity is important to maximizing the utility especially when battery is in a low state of charge. For example, when the battery state of charge (SOC) at 0.1C is 0.2 and  $\theta=1$ , the optimal CPU supply voltage determined by the MRC and MCC methods are 1.13V and 1.23V, respectively. However, by using the Mopt method, the actual optimal CPU voltage is found to be 1.05V. In this case, the Mopt method achieved 15% improvement over the MRC method in terms of the total utility. For the same setup, the MCC method yielded 31% lower total utility even compared to the MRC method.

**Table I**  
**SIMULATION RESULTS FOR OPTIMAL VOLTAGE SETTING**

Battery SOC at 0.1C	$\theta$	MRC	Mopt		MCC	
		Vopt	Util	Vopt	Util	Vopt
0.9	0.5	1.01	1.00	1.01	1.00	1.03
	1	1.13	1.00	1.13	0.91	1.23
	1.5	1.22	1.00	1.22	0.98	1.26
0.5	0.5	1.01	1.00	1.00	0.98	1.03
	1	1.13	1.01	1.10	0.86	1.23
	1.5	1.22	1.01	1.19	0.97	1.26
0.3	0.5	1.01	1.01	0.99	0.97	1.03
	1	1.13	1.06	1.07	0.78	1.23
	1.5	1.22	1.06	1.15	0.95	1.26
0.2	0.5	1.01	1.04	0.98	0.95	1.03
	1	1.13	1.15	1.05	0.69	1.23
	1.5	1.22	1.19	1.11	0.98	1.26
0.1	0.5	1.01	1.16	0.96	0.91	1.03
	1	1.13	1.59	1.01	0.49	1.23
	1.5	1.22	1.86	1.05	0.64	1.26

### III. BATTERY BACKGROUND

This paper focuses on lithium-ion batteries because they are the fastest growing battery systems. Lithium-ion batteries are widely used in the notebook computers and cellular phones due to the high energy density and light weight. The schematic of the lithium-ion battery under consideration (Bellcore's PLION battery) in this paper is shown in Figure 1. It consists of the positive electrode ( $Li_yMn_2O_4$ ), negative electrode ( $Li_xC_6$ ) and a plasticized electrolyte composed of a 1M LiPF6 in EC/DMC in a silica-tiled p(VdF-HFP) copolymer matrix. The current collectors are made of aluminum (positive) and copper (negative) [20].

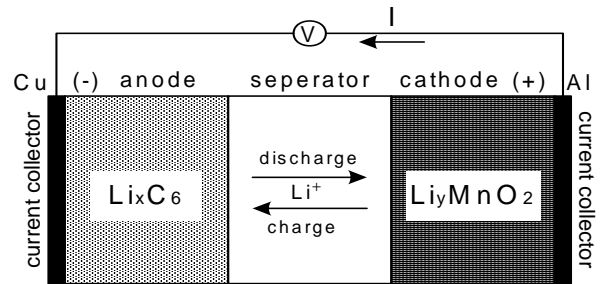
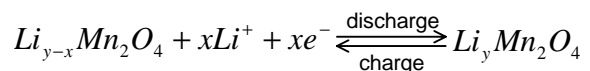


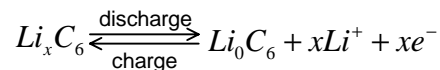
**Figure 2. Schematic of a lithium-ion battery.**

The electrochemical reactions at the electrodes are [4]:

At positive electrode (cathode):



At negative electrode (anode):



During the discharge process lithium ion de-inserts from solid particles of the negative electrode and inserts into solid

particles of the positive electrode. The process is reversed during the charge process.

Cell discharge is limited mainly by two mechanisms: lithium ion diffusion in the solid phase and electrolyte depletion in the positive electrode. Usually, an end of discharge is considered to have been reached when the cell potential drops below a threshold, called the cut-off voltage.

A rechargeable battery may regain its capacity through the charge process. A discharge and the following charge are called a cycle. The deliverable capacity of a lithium-ion battery tends to decrease as the cycle count increases. This phenomenon is called cycle aging phenomena.

In the following sub-sections, we will introduce the basic equations related to the battery inner electrochemical processes.

#### A. Notation

The following notation is used in the remainder of this paper.

##### General

- $c$  : Concentration
- $E_a$  : Activation energy
- $F$  : Faraday's constant, 96,485C mol<sup>-1</sup>
- $\mathcal{K}$  : Conductivity
- $i_o$  : Exchange current density
- $R$  : Gas constant, 8.3144 J K<sup>-1</sup> mol<sup>-1</sup>
- $n$  : Number of electrons transferred
- $\alpha$  : Transfer coefficient

##### Superscripts

- $b$  : Bulk
- $s$  : Surface of electrode

##### Subscripts

- $a$  : Anode
- $c$  : Cathode
- $r$  : Reactant consumed in the oxidation reaction
- $o$  : Reactant consumed in the reduction reaction

#### B. Cell Potential

Cell potential does not represent a source of energy, rather it denotes a voltage drop inside the battery during its discharge process due to the physical and chemical changes in the properties of the material that make up the battery electrodes and electrolyte. The overall cell potential may be divided into three parts [21][22]: the ohmic overpotential  $\eta_{ohm}$ , the surface overpotential  $\eta_s$ , and the concentration overpotential  $\eta_c$ .

Based on Ohm's law, Ohmic overpotential  $\eta_{ohm}$  can be expressed as an integral from the cathode to the anode:

$$\eta_{ohm} = IR_{soln} = \frac{iA(0)}{\mathcal{K}} \int_0^L \frac{dx}{A(x)} \quad (3-1)$$

where  $R_{soln}$  is the resistance between the two electrodes,  $A(x)$  is the area of the cross-section at distance  $x$  from the negative electrode, and  $L$  is the distance between the two electrodes.

$\eta_s$  is the potential that makes the electrode reactions proceed at appreciable rates. It is related to the current density, which is governed by the following equation:

$$i = i_0 \left[ \exp\left(\frac{\alpha_a F}{RT} \eta_s\right) - \exp\left(-\frac{\alpha_c F}{RT} \eta_s\right) \right] \quad (3-2)$$

where  $T$  is temperature in Kelvin and  $i_0$  is the exchange current density. If oxidation reaction is dominant in the anode and reduction reaction is dominant in the cathode, then the above equation can be reduced to:

$$\eta_{s,a} = \frac{RT}{\alpha_a F} \ln \frac{i}{i_{0,a}}, \quad \eta_{s,c} = -\frac{RT}{\alpha_c F} \ln \frac{i}{-i_{0,c}} \quad (3-3)$$

for the anode and cathode, respectively

$\eta_c$  is caused by the concentration variations near the surface of the electrode. In solutions with an excess of supporting electrolytes, it can be approximated as:

$$\eta_{c,a} = \frac{RT}{nF} \ln \frac{c_r^b}{c_r^s}, \quad \eta_{c,c} = \frac{RT}{nF} \ln \frac{c_o^b}{c_o^s} \quad (3-4)$$

at the anode and cathode, respectively.

#### C. Temperature Dependence

The transport and kinetic properties usually exhibit an Arrhenius dependence on temperature, which is described by the following equation [4]:

$$\Phi = \Phi_{ref} \exp\left[\frac{E_a(\Phi)}{R} \left(\frac{1}{T_{ref}} - \frac{1}{T}\right)\right] \quad (3-5)$$

where  $\Phi$  is a generic variable representing any of the following parameters the diffusion coefficient of a species, conductivity of the electrolyte  $\mathcal{K}$ , exchange current density of an electrode reaction, etc., and subscript *ref* denotes the value at a reference temperature.  $E_a(\Phi)$  is the activation energy of the evolution process of  $\Phi$ . Its magnitude determines the sensitivity of  $\Phi$  to temperature.

#### D. Cycle Aging

The cycle aging phenomenon of lithium-ion batteries involves several different side reactions, such as cell oxidation processes, electrolyte decomposition (reduction) processes and self-discharge processes [23]. According to [24], the loss of charge acceptance of the Lithium-ion batteries is mainly due to cell oxidation, which occurs naturally during use and as a part of aging. The cell oxidation leads to a film grown on the electrode, which non-reversibly increases the internal resistance of lithium-ion batteries and finally causes a failure. Usually, it is adequate to describe the film growth using a

linear approximation. In [23], the growth of the film is related to the rate of the side reaction by

$$\frac{\partial \delta}{\partial t} = \frac{i_k M}{L \alpha \rho F} \quad (3-6)$$

where  $\delta$  is the film thickness composed of lithium products,  $i_k$  is the rate (current) of the side reaction, other parameters  $M, L, a, \rho, F$  are all constant for a given reaction and a given battery.

#### IV. MODEL DESCRIPTION

The objective of this paper is to construct a high-level model to predict the remaining capacity of a rechargeable lithium-ion battery in terms of the battery output voltage, discharge-rate (current), battery temperature, and the cycle age of the battery. Here the term current always means that the average current at which the battery is supposed to be discharged to its end of life starting from this point in time.

##### A. Modeling the Cell Terminal Voltage

During the discharge process, the output terminal voltage  $v$  is equal to the initial open-circuit voltage  $VOC_{init}$  minus the voltage drop inside the battery, which is in turn caused by the drained current. This voltage drop is also known as the cell potential. It is denoted by  $\eta$  and is calculated as:

$$\eta = \eta_{ohm} + (\eta_{s,a} - \eta_{s,c}) + (\eta_{c,a} - \eta_{c,c}) \quad (4-1)$$

From (3-2) and (3-3), one can see that if the discharged current is constant, the first two overpotential terms in (4-1) are also constant and do not vary with time. So one can use a resistance to represent the effect of these two overpotentials:

$$r(i, T) = a_1(T) + \frac{a_2(T) \ln i}{i} + \frac{a_3(T)}{i} \quad (4-2)$$

where,

$$a_1(T) = \frac{A(0)}{\kappa} \int_0^L \frac{dx}{A(x)}$$

$$a_2(T) = \frac{RT}{F} \left( \frac{1}{\alpha_a + \alpha_c} \right)$$

$$a_3(T) = \frac{RT}{F} \left( -\frac{\ln i_{0,a}}{\alpha_a} + \frac{\ln(-i_{0,c})}{\alpha_c} \right). \quad (4-3)$$

Based on (3-4), the concentration overpotential term in (4-1) is

$$\eta_{c,a} - \eta_{c,c} = \frac{RT}{nF} \ln \frac{c_{r,a}^b c_{o,c}^b}{c_{r,a}^s c_{o,c}^s}. \text{ At the very beginning of the}$$

discharge process, the concentration near the electrode surface should be the same as the concentration in the bulk solution. As the charge is drained off the battery, the concentration near the electrode surface decreases while the bulk concentration remains almost unchanged. So the ratio of surface concentration to the bulk concentration is approximated by

$1 - b_1 \cdot c^{b_2}$ , where  $c$  is the charge capacity delivered up to this point. Also it's assumed that the form  $1 - b_1 \cdot c^{b_2}$  applies to the both electrodes. Thus, the concentration overpotential can be expressed as:

$$\eta_{c,a} - \eta_{c,c} = -\lambda \ln(1 - b_1(i, T) \cdot c^{b_2(i, T)}) \quad (4-4)$$

where  $\lambda = \frac{2RT}{nF}$  and  $b_1$  and  $b_2$  are functions of discharge-rate and temperature, respectively.

Now a closed form expression for  $v$  may be written as:

$$v(c, i, T) = VOC_{init} - r(i, T) \cdot i + \lambda \cdot \ln(1 - b_1(i, T) \cdot c^{b_2(i, T)}). \quad (4-5)$$

##### B. Modeling the Temperature Dependence

When temperature varies among different cycles, one needs to take into account the temperature dependence of model-related properties of the battery material, such as electrolyte conductivity, electrolyte diffusion coefficients, and rate of electrochemical reactions.

By considering the Arrhenius dependence  $\kappa$  (c.f. section 3.3) of conductivity, based on (4-3),  $a_1$  is expected to be related to  $T$  by:

$$a_1(T) = a_{11} \cdot \exp\left(\frac{a_{12}}{T}\right) + a_{13} \quad (4-6)$$

where,  $a_{11}, a_{12}, a_{13}$  are all constant, among which  $a_{13}$  is an introduced parameter that helps calibrate the prediction.

Since  $\alpha_a$  and  $\alpha_c$  are unrelated to the temperature  $T$ , from (4-3), it is known that  $a_2$  should be linearly proportional to the  $T$ :

$$a_2(T) = a_{21}T + a_{22} \quad (4-7)$$

where,  $a_{21}, a_{22}$  are constant.

In addition, if one considers the Arrhenius dependence of exchange current density  $i_{0,a}$  and  $i_{0,c}$ , one can get the temperature dependence for  $a_3$  from (4-3):

$$a_3(T) = a_{31}T^2 + a_{32}T + a_{33} \quad (4-8)$$

where,  $a_{31}, a_{32}, a_{33}$  are all constant.

Using the same analytical method, when considering the Arrhenius temperature dependence of the diffusion coefficient of the active material, one can find that:

$$b_1(i, T) = d_{11} \exp\left(\frac{d_{12}}{T}\right) + d_{13} \quad (4-9)$$

$$b_2(i, T) = \left( \frac{d_{21}}{T + d_{22}} \right) + d_{23} \quad (4-10)$$

where  $d_{11}$  to  $d_{23}$  are functions of current  $i$ . In this paper, based on our curve fitting, we assume that their dependencies on the current are as follows:

$$d_{jk}(i) = \sum_{z=0}^4 m_z(d_{jk}) \cdot i^z \quad (4-11)$$

where,  $j=1,2$ ,  $k=1,2,3$  and  $m_z(d_{jk})$  are constant coefficients.

### C. Modeling the Cycle Aging

Based on Ohm's law, the resistance of the film grown on the electrode surface  $r_f$  is proportional to its thickness,  $\Delta r_f \propto i_k \cdot \Delta t$ . Based on the above formula, it is reasonable to assume that  $\Delta r_f$  is proportional to  $\Delta C$ , which is the capacity delivered during  $\Delta t$ . If during each cycle the total capacity delivered is roughly the same, then  $r_f$  can be considered as a linear function of  $n_c$ , the number of cycles that the battery has experienced before.

The temperature also has a significant impact on the film growth. More precisely, the cycle life of a battery decreases as temperature increases. In [20], authors claimed that their lithium-ion battery could survive more than 2000 cycles at  $25^\circ C$  but only 800 cycles at  $55^\circ C$ . As stated in [22], this is due to the Arrhenius dependence of reaction rate  $i_k$  on temperature. So  $r_f(n_c, T')$  is described as follows:

$$r_f(n_c, T') = k \cdot n_c \cdot \exp\left(-\frac{e}{T'} + \psi\right) \quad (4-12)$$

where  $k$  is a constant,  $e = E_a$ ,  $\psi = \frac{E_a}{T'_{ref}}$ , and  $T'$  is the

temperature that the battery experienced in the previous cycles.

Combining (4-12) and (4-2), the expression of  $r$  in (4-5) is rewritten to include the cycle aging effect,

$$r(i, T, n_c, T') = r_0(i, T) + r_f(n_c, T') \quad (4-13)$$

where,  $r_0(i, T)$  represents the original form derived in (4-2).

If the battery experienced different temperatures in the previous cycles, a probability distribution can be used to describe the temperature history. Let  $P(T')$  denote the probability that the temperature is  $T'$  in some cycle. The film resistance can be expressed as:

$$r_f(n_c, T') = n_c \cdot \sum_{T'} P(T') \cdot k \exp\left(-\frac{e}{T'} + \psi\right) \quad (4-14)$$

### D. Computing the Remaining Capacity

*State of charge* (SOC) is a widely used concept in the literature to represent the remaining capacity of a battery in a charge/discharge cycle. It is defined as the ratio of the *remaining capacity* (RC) to the *full charge capacity* (FCC). However, due to the cycle aging phenomenon, using SOC alone may result in large errors because the FCC of a cycle-aged battery may be significantly less than the *design capacity* (DC) that denotes the FCC of a newly manufactured battery. Considering the cycle aging effect, a new concept, *state of health* (SOH) is defined as the ratio of FCC of cycle-aged battery to its DC. Using the equation derived in the above subsections, we can obtain equations for SOC and SOH.

Equation (4-5) can be reformulated as:

$$b_1(i, T) \cdot c^{b_2(i, T)} = 1 - \exp\left(\frac{r(i, T, n_c, T') \cdot i - (VOC_{init} - v)}{\lambda}\right) \quad (4-15)$$

To simplify the notation, let  $r_0 = r(i, T, 0, T')$ ,  $r_n = r(i, T, n_c, T')$ ,  $\Delta v = VOC_{init} - v$  and  $\Delta v_m = VOC_{init} - v_{cut-off}$  and use  $b_1$  and  $b_2$  to represent  $b_1(i, T)$  and  $b_2(i, T)$ .

Using equation (4-15), SOH and DC are computed as:

$$DC = \left\{ \frac{1}{b_1} \left[ 1 - \exp\left(\frac{r_0 \cdot i - \Delta v_m}{\lambda}\right) \right] \right\}^{\frac{1}{b_2}} \quad (4-16)$$

$$SOH = \frac{\left[ 1 - \exp\left(\frac{r_n \cdot i - \Delta v_m}{\lambda}\right) \right]^{\frac{1}{b_2}}}{\left[ 1 - \exp\left(\frac{r_0 \cdot i - \Delta v_m}{\lambda}\right) \right]^{\frac{1}{b_2}}} \quad (4-17)$$

From (4-15), (4-16) and (4-17), SOC can be related to SOH and DC as follows:

$$SOC = 1 - \frac{\left[ \frac{1}{b_1} - \left( \frac{1}{b_1} - SOH^{b_2} \cdot DC^{b_2} \right) \exp\left(\frac{\Delta v_m - \Delta v}{\lambda}\right) \right]^{\frac{1}{b_2}}}{SOH \cdot DC} \quad (4-18)$$

Finally, RC is calculated as:

$$RC = SOC \cdot SOH \cdot DC \quad (4-19)$$

This last equation (4-19) in combination with equations (4-16), (4-17) and (4-18) is the key result of the present paper. It is a completely new result.

### E. Determining Model Parameters

Before using the model presented here, the related parameters need to be determined. All parameters can be obtained from the battery experimental data. For example,  $r(i, T)$  in (4-5) is equal to the initial battery potential drop

divided by the current. When the values of  $r(i, T)$  are obtained, the parameters to be determined can be divided into two parts.  $b_1$  and  $b_2$  may be obtained by finding an optimum fit of equation (4-5) to the battery voltage-discharged capacity trace using the least squares fitting method.  $a_1$  to  $a_3$  are determined using the same fitting method to fit equation (4-6,7,8) to the values of  $r(i, T)$ . Because  $b_1$ ,  $b_2$  and  $a_1$  to  $a_3$  are known, values of other model parameters that are dependent on them can be calculated in a similar way: step by step, until all parameter values are found.

## V. MODEL VALIDATION

### A. Experimental Setup

The DUALFOIL program [3] is used to simulate a Bellcore's PLION battery [20]. The parameters are set up according to [25].

#### 1. Setup for cycle life simulation

The original form of the DUALFOIL does not support the cycle aging effect. After private correspondence with the authors of the DUALFOIL, the code was modified to incorporate a capacity degradation mechanism. The modified DUALFOIL was verified with the actual cycle-life data provided in [20]. Comparison between the simulation results and the actual battery data for a battery temperature of  $22^\circ\text{C}$  is shown in Figure 1. The maximum error of the full discharged capacity is less than 2%.

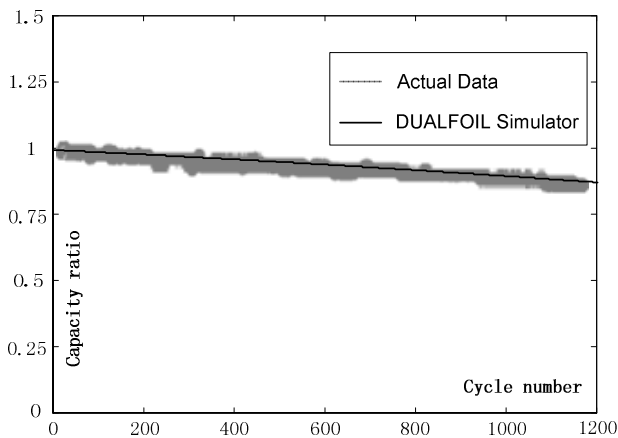


**Figure 3. Battery capacity fading data as a function of Battery cycle life ( $T = 22^\circ\text{C}$ ).**

#### 2. Setup for temperature effect simulation

The original form of the DUALFOIL does not specify the temperature dependence of the material properties, i.e., temperature only appears in the diffusion potential term of the modified Ohm's law in the electrolyte and in the Butler-Volmer equation. Without accounting for the temperature dependencies of the material properties, the simulation results contradict the actual battery experimental data.

We adopted the thermal model developed in [26], which was originally developed to predict the temperature behavior of lithium/polymer battery. This thermal model is a variation of the DUALFOIL model with the addition of energy balance equation and physical property variations with temperature. The related thermal parameters in the model are adjusted to match the experimental data for the materials used in the PLION battery. For example, the fitted temperature dependence of the ionic conductivity is shown in Figure 4, where the circle points denote the conductivity values measured in [27] for the electrolyte 1M LiPF<sub>6</sub>/EC/DMC in PVdF-HFP. The temperature dependences of the properties involved in the film growth were estimated according to the cycle-life data provided in [20].

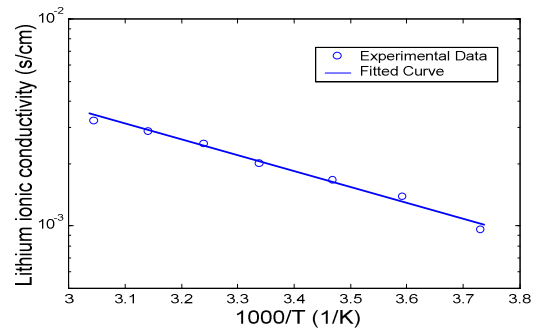


**Figure 4. Lithium ionic conductivity of 1M LiPF<sub>6</sub>/DC/EMC in PVdF.**

### B. Experimental Results

To determine the model parameters, a wide range of battery working conditions were simulated.

Temperature range:

$$\{-20^\circ\text{C}, -10^\circ\text{C}, 0^\circ\text{C}, 10^\circ\text{C}, 20^\circ\text{C}, 30^\circ\text{C}, 40^\circ\text{C}, 50^\circ\text{C}, 60^\circ\text{C}\}$$

During this simulation, it was assumed that the battery is always working at the same temperature, which means that the temperature in the previous cycle is the same as that in the current cycle.

Discharged current range:

$$\left\{ \frac{C}{15}, \frac{C}{6}, \frac{C}{3}, \frac{C}{2}, \frac{2C}{3}, \frac{5C}{6}, C, \frac{7C}{6}, \frac{4C}{3} \right\}, \text{ where the "1C" rate}$$

denotes a rate at which a fresh fully charged battery will be discharged to exhaustion in an hour at room temperature. For the battery examined in this paper, "1C" is equal to  $41.5\text{mA}$ .

Cycle number range: up to 1,200 cycles or SOH below 80%.

The discharge profile at any combination of abovementioned temperature, discharge current and cycle number (the hundredths only) was obtained. The obtained model parameters are listed in Table 1. The full discharged capacity of the battery at  $C/15$  and at  $20^\circ\text{C}$  is taken as a unity when calculating the remaining capacity prediction error. The max prediction error is less than 6.4% and the average prediction error is 3.5%. Secondly, we performed the following tests to examine the proposed model.

Test case 1) The battery was cycled to 1200 cycles at “1C” rate at 20°C. The SOC profiles of the 200th, 475th, 750th and 1025th cycles are compared with the predictions of the proposed model in Figure 3.

Test case 2) The battery was cycled to 200 cycles at 20°C. The discharge current of each cycle was assumed to be uniformly distributed in the range of C/15 to 4C/3. Next the battery was discharged at C/3, 2C/3 and C, and at 0°C, 20°C and 40°C. The remaining capacity profiles were compared with those predicted by the proposed model in Figure 4. The max prediction error is 4.2%.

Test case 3) The battery was cycled to 360 cycles at “1C” rate. The temperature of each cycle was assumed uniformly distributed in the range from 20°C to 40°C. Next the battery was discharged at C/15 and 1C at 20°C. The simulation results were compared with the predictions of the proposed model in Figure 5. The max remaining capacity prediction error is 4.9%.

## VI. ONLINE ESTIMATION OF A BATTERY’S REMAINING CAPACITY

### A. System Architecture

The structure of an electronic system integrating the support of system management bus (SMBus) [24] for the battery source is shown in Figure 5. (The SMBus battery is also known as “smart battery”.) The SMBus is a two-wire interface system developed on Inter-IC (I<sup>2</sup>C) bus technique, which is a synchronous bi-directional communications system with an interface comprising of a clock wire and a data wire. It operates at a rate of up to 100 KHz. The SMBus circuit is integrated inside the battery, which consists of voltage/current and temperature sensors with corresponding AD converters. Through the SMBus, the internal measured battery data can be transferred to the outside power manager, which can then adjust the performance/power dissipation behavior of the electronic system.

A data flash memory can also be integrated into the SMBus circuit, which provides storage for manufacturing data and temporary buffer for the user acquired data, such as instantaneous voltage and/or current measurement, accumulated coulomb counting, cycle counting, and so on. When the power manager obtains the battery data, it invokes the software module to analyze and handle the data based on battery model, and predict the battery remaining capacity and lifetime.

### B. Online Prediction Methods

The first method we consider is a simple method based only on current-voltage measurement and is thus referred as the IV method. The use of this method only requires the battery output terminal voltage given that the battery will be discharged at the current rate. At any time instant  $t$ , if we know the terminal voltages,  $v_1$  and  $v_2$ , for different currents  $i_1$  and  $i_2$ , then the terminal voltage at current  $i$  at time  $t$  can be calculated as

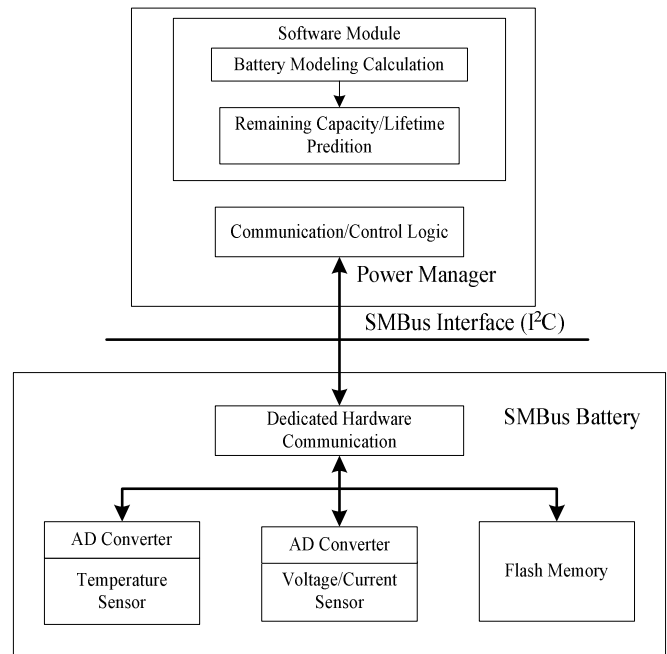


Figure 5. Architecture of an electronic system with SMBus support.

$$v = \frac{v_1 - v_2}{i_1 - i_2} i + v_2 . \quad (6-1)$$

This equation holds because only the ohmic overpotential can change instantly. By substituting the terminal voltage into equation (4-19) with the current, temperature and cycle age information, we can obtain the battery’s remaining capacity. This method is quite accurate when a battery is discharged at a constant current rate. However, in an environment where a battery works with a variable load, this method may produce large errors due to the non-ideal characteristics of a battery. To address this shortcoming, we describe below a more elaborate method which incorporates the discharge history to adjust the prediction.

In this section, we consider the problem of battery’s remaining capacity prediction as defined as follows: Predict the remaining capacity of a battery at time  $t$ , given that an initial fully-charged battery has been discharged at a constant rate  $i_p$  from time 0 to  $t$ . However, after time  $t$ , the battery is expected to be discharged to exhaustion at another constant rate  $i_f$ . In practice, the value of  $i_f$  may be estimated based on the application running on the processor. Some level of static profiling [28] or compiler level annotation [29] will be helpful to improve accuracy of this prediction, which falls outside the scope of the present paper.

Let  $RC^{IV}$  denote the prediction made by the IV method, which is calculated by using equation (4-19) with current  $i_f$  substituted for  $i$ . Consequently,  $RC^{IV}$  can be expressed as

$$RC^{IV} = SOC(i_f)FCC(i_f) \quad (6-2)$$

where  $FCC(i_f)$ , as was defined in section 4.4, represents the full deliverable capacity as though the battery is constantly discharged at rate  $i_f$  in the present discharge cycle.

To incorporate the discharge history, we consider adjusting the prediction made by the IV method by using a coulomb counting method, which is referred to as the CC method. The CC method predicts the battery remaining capacity by using the following equation

$$RC^{CC} = FCC(i_f) - i_p t. \quad (6-3)$$

The actual prediction by the resulting method is a linear combination of the predictions by the IV and CC methods, i.e.,

$$RC = \gamma RC^{IV} + (1 - \gamma) RC^{CC}, \quad (6-4)$$

where  $\gamma$  is determined according to the rules presented below. Let  $n_c$  denote the cycle age of the battery and  $T$  the discharge temperature.

1)  $i_f < i_p$

$$\gamma = \gamma_c(T, r_f, n_c) \frac{i_p^2 i_f t}{\sqrt{i_p - i_f}}, \quad (6-5)$$

where  $\gamma_c$  is a coefficient whose value can be read from a table indexed by  $T$  and  $r_f$ . This table is generated offline by fitting the calculated  $\gamma$  with the actual simulated values.

2)  $i_f > i_p$

$$\gamma = (i_p + \gamma_{c1})(\gamma_{c2} i_f + \gamma_{c3}), \quad (6-6)$$

where  $\gamma_{c1}$ ,  $\gamma_{c2}$  and  $\gamma_{c3}$  are coefficients whose values can be read from a table indexed by  $T$  and  $r_f$ . This table is also generated offline by using a curve fitting method.

We performed experiments to examine the prediction accuracy of different methods. The experiments were performed for over 3240 instances; the tested configurations corresponded to a combination of temperature (5°C, 25°C, 45°C), cycles (300<sup>th</sup>, 600<sup>th</sup>, 900<sup>th</sup>) and all valid combinations of currents in the set shown in section 5.2 with 10 discharge states each. In the case where  $i_f < i_p$ , the average prediction error is 1.03% whereas the maximum error is less than 2.94%. In the second case, the average prediction error is 3.48% while the maximum error is less than 12.6%. Notice that the full discharged capacity of the battery at C/15 and at 20°C is taken as unity when calculating the remaining capacity prediction error.

### C. Revisiting the DVFS Application

Let's re-consider the motivating application of section 2; the experimental setup remains the same. However, this time we use the battery remaining capacity estimated by using the method presented in section 6.2 in order to calculate the optimal supply voltage for the Xscale processor. After that, simulations were performed to determine the actual obtained utilities when the Xscale processor runs at the calculated supply voltages. The simulation results are presented in Table

II under method "Mest", which are very close to the optimal results, "Mopt".

**Table II.**  
**Simulation results for optimal voltage setting**

Battery SOC at 0.1C	$\theta$	Mopt		Mest	
		Util	Vopt	Util	Vopt
0.9	0.5	1.00	1.01	1.00	1.02
	1	1.00	1.13	1.00	1.13
	1.5	1.00	1.22	1.00	1.22
0.5	0.5	1.00	1.00	1.00	1.01
	1	1.01	1.10	1.01	1.11
	1.5	1.01	1.19	1.01	1.19
0.3	0.5	1.01	0.99	1.01	1.00
	1	1.06	1.07	1.06	1.08
	1.5	1.06	1.15	1.06	1.14
0.2	0.5	1.04	0.98	1.03	0.98
	1	1.15	1.05	1.14	1.04
	1.5	1.19	1.11	1.16	1.08
0.1	0.5	1.16	0.96	1.14	0.95
	1	1.59	1.01	1.42	0.97
	1.5	1.86	1.05	1.47	0.99

## VII. CONCLUSION

A comprehensive high-level model was presented to predict the remaining capacity of a battery considering the temperature effect and the cycle aging effect. The effectiveness of this model was validated by comparing it with detailed battery simulation results. Techniques based on this model were developed for online prediction of the remaining battery capacity under variable workload conditions. The use of this model for dynamic power management was demonstrated through a DVFS application scenario.

**Table III**  
**Parameters of the proposed high-level battery model**

Parameter Name		Value				
	$\lambda$	0.43				
$a_1$	$a_{11}$	$a_{12}$	$a_{13}$			
	-0.438	2.10	0.448			
$a_2$	$a_{21}$	$a_{22}$				
	-4.1e-3	0.64				
$a_3$	$a_{31}$	$a_{32}$	$a_{33}$			
	-3.82e-6	2.4e-3	-0.368			
$b_1$	$d_{11}$	$m_4$	$m_3$	$m_2$	$m_1$	$m_0$
		1.91e-9	-2.28e-7	8.36e-6	-8.77e-5	1.92e-4
$d_{12}$	$d_{12}$	$m_4$	$m_3$	$m_2$	$m_1$	$m_0$
		-2.04e-3	0.24	-9.15	99.7	1.82e3
$d_{13}$	$d_{13}$	$m_4$	$m_3$	$m_2$	$m_1$	$m_0$

	-8.51e-8	9.49e-6	-3.10e-4	3.13e-3	0.135
$d_{21}$	$m_4$	$m_3$	$m_2$	$m_1$	$m_0$
	1.83e-4	-1.96e-2	0.571	-1.46	5.97
$b_2$	$m_4$	$m_3$	$m_2$	$m_1$	$m_0$
	4.67e-5	4.88e-3	0.135	-0.451	-2.24e2
$d_{23}$	$m_4$	$m_3$	$m_2$	$m_1$	$m_0$
	-1.14e-6	1.13e-4	-2.73e-3	-3.84e-3	2.07
$k$				1.17e-4	
$e$				2.69e3	
$\psi$				9.02	

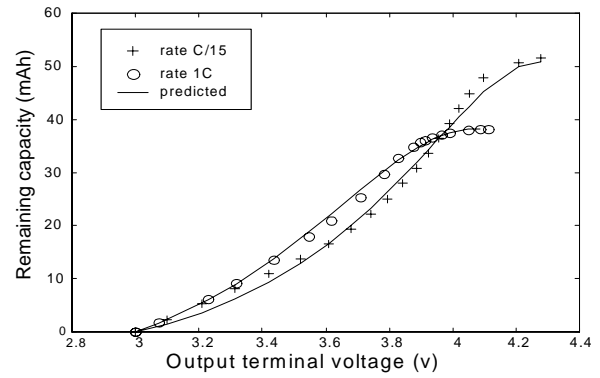


Figure 8. Remaining capacity traces for test case (3).

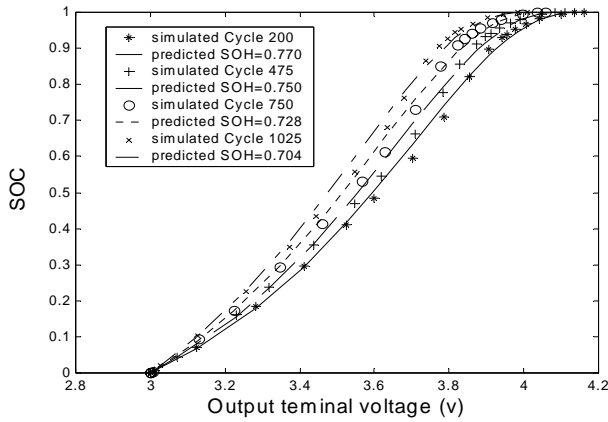


Figure 6. SOC traces for test case (1).

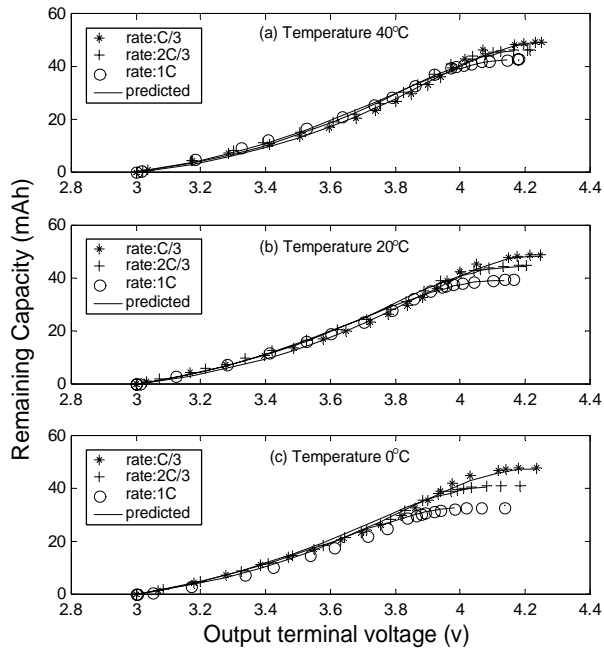


Figure 7. Remaining capacity traces for test case (2).

REFERENCES

- [1] M. Pedram and Q. Wu, "Design considerations for battery-powered electronics," *Proc. 36th Design Automation Conf.*, pp. 861-866, Jun. 1999.
- [2] K. Lahiri, A. Raghunathan, S. Dey and D. Panigrahi, "Battery-driven system design: a new frontier in low power design," *Proc. ASP-DAC*, pp. 261-267, Jan. 2002.
- [3] M. Doyle, T.F. Fuller, and J. Newman, "Modeling of galvanostatic charge and discharge of the lithium/polymer/insertion cell," *J. Electrochem. Soc.*, Vol. 141, No. 1, pp. 1-9, Jan. 1994.
- [4] W.B. Gu and C.Y. Wang, "Thermal and electrochemical coupled modeling of a Lithium-ion cell in Lithium batteries," *Proceedings of ECS*, Vol.99-25 (1), pp.748-762, 2000.
- [5] S. Gold, "A PSPICE macromodel for lithium-ion batteries," *Battery Conference on Applications and Advances*, pp. 215-222, 1997.
- [6] L. Benini et al., "Discrete-time battery models for system-level low-power design," *IEEE Trans. VLSI Systems*, vol. 9, no. 5, pp. 630-640, 2001.
- [7] M. Pedram and Q. Wu, "Battery-powered digital CMOS design," *IEEE Trans. VLSI Systems*, vol. 10, no. 5, pp. 601-607, 2002.
- [8] D.Panigrahi, C.Chiasserini, S.Dey, R.Rao, A.Raghunathan, K.Lahiri, "Battery Life Estimation for Mobile Embedded Systems," *Proc. Intl. Conf. on VLSI Design*, pp.55-63, Bangalore, January 2001.
- [9] D. Rakhmatov and S. B. K. Vrudhula, "An Analytical High-Level Battery Model for use in Energy Management of Portable Electronic Systems," *Proc. IEEE Int'l Conf. on Computer Aided Design*, pp. 488-493, Nov. 2001.
- [10] R. Rao, S. Vrudhula and D. Rakhmatov, "Battery Modeling for Energy-Aware System Design," *Computer*, Vol. 36, No. 12, pp. 77-87 Dec. 2003.
- [11] B.A. Johnson and R.E. White, "Characterization of commercial available lithium-ion batteries," *Journal of Power Sources*, Vol.70, Iss.1, pp 48-54, Jan. 1998.
- [12] Simmonds et al., Device for indicating the residual capacity of secondary cells, *U.S. Patent*, no. 5479085, 1995.
- [13] Kozaki, Remaining battery capacity meter and method for computing remaining capacity, *U.S. Patent*, no. 5691078, 1997.
- [14] F. Huet, A review of impedance measurements for determination of the state of charge or state of health of secondary batteries, *J. Power Sources*, vol. 70, pp. 59-69, 1998.
- [15] S. Shenker, "Fundamental Design Issues for the Future Internet," *IEEE Journal on Selected Areas in Communications*, 13:1176-88, Sept. 1995.

- [16] C. Zhou, D. Qian and H. Lee, "Utility-based routing in wireless ad hoc networks," *Proc. IEEE Intl. Conf. on Mobile Ad-hoc and Sensor Systems*, pp. 588-593, Oct. 2004.
- [17] W.E Walsh, G. Tesauro, J.O Kephart and R. Das, "Utility functions in autonomic systems," *Proc. Intl. Conf. on Autonomic Computing*, pp. 70-77, May 2004.
- [18] T. Martin, "Balancing batteries, power and performance: System issues in CPU speed-setting for mobile computing," Ph.D. Dissertation, Carnegie Mellon University, Department of Electrical and Computer Engineering, Aug. 1999.
- [19] K. Choi, R. Soma and M. Pedram, "Fine-Grained Dynamic Voltage and Frequency Scaling for Precise Energy and Performance Trade-off based on the Ratio of Off-chip Access to On-chip Computation Times," *Proc. of Design Automation and Test in Europe*, pp. 4-9, Feb. 2004.
- [20] J.M. Tarascon, A.S. Gozdz, C. Schmutz, F. Shokoohi, and P.C. Warren, "Performance of bellcore's plastic rechargeable Li-ion batteries," *Solid State Ionics*, pp 49-54, Month: 1996.
- [21] H.B. Oldham, J.C. Myland, *Fundamentals of Electrochemical Science*, San Diego, Academic Press, Inc. 1994.
- [22] J.S. Newman, *Electrochemical Systems*, 2nd ed., New Jersey, Prentice Hall, 1991.
- [23] P. Arora, R.E. White, "Capacity fade mechanisms and side reactions in lithium-ion batteries," *J. Electrochem. Soc.*, Vol. 145, No. 10, pp. 3647-67, October 1998.
- [24] I. Buchmann, *Batteries in a Portable World*, URL: <http://www.buchmann.ca/toc.asp>.
- [25] P. Arora, M. Doyle, A.S. Gozdz, R. E. White, and J. Newman, "Comparison between computer simulations and experimental data for high-rate discharges of plastic lithium-ion batteries," *Proc. Electrochemical Society*, 1998, Vol.10, pp. 29-45.
- [26] C.R. Pals, J.S. Newman, "Thermal modeling of the lithium/polymer battery. I. discharge behavior of a single cell," *J. Electrochem. Soc.*, Vol 142, No. 10, pp. 3274-81, October 1995.
- [27] J.Y. Song, "Electrochemical study of microporous polymer electrolytes based on poly (vinylidene fluoride) copolymer", Ph.D. dissertation, June 2000.
- [28] K. Lahiri, A. Raghunathan, and S. Dey, "Efficient power profiling for battery-driven embedded system design" *IEEE Trans on CAD*, Vol 23, Iss 6, pp. 919-932, June 2004.
- [29] C. Brandolese, W. Fornaciari, L. Pomante, F. Salice, D. Sciuto, "A multi-level strategy for software power estimation," *Intl. Symp. On System Synthesis*, pp. 187-192, Sept. 2000.



**Peng Rong** (S'02) received B.S. and M.S. degree in Electronic Engineering from Tsinghua University, China in 1998 and 2001, respectively. He has been pursuing a Ph.D. degree in Electrical Engineering at the University of Southern California since 2001. His research interests are in the area of system-level power management and low-power design.



**Massoud Pedram** (S'88-M'90-SM'98-F'01) received a B.S. degree in Electrical Engineering from the California Institute of Technology in 1986 and M.S. and Ph.D. degrees in Electrical Engineering and Computer Sciences from the University of California, Berkeley in 1989 and 1991, respectively. He then joined the department of Electrical Engineering - Systems at the University of Southern California where he is currently a professor.

Dr. Pedram has served on the technical program committee of a number of conferences, including the Design automation Conference (DAC), Design and

Test in Europe Conference (DATE), Asia-Pacific Design automation Conference (ASP-DAC), and International Conference on Computer Aided Design (ICCAD). He served as the Technical Co-chair and General Co-chair of the International Symposium on Low Power Electronics and Design (SLPED) in 1996 and 1997, respectively. He was the Technical Program Chair and the General Chair of the 2002 and 2003 International Symposium on Physical Design. Dr. Pedram has published four books and more than 300 journal and conference papers. His research has received a number of awards including two ICCD Best Paper Awards, a Distinguished Citation from ICCAD, a DAC Best Paper Award, and an IEEE Transactions on VLSI Systems Best Paper Award. He is a recipient of the NSF's Young Investigator Award (1994) and the Presidential Faculty Fellows Award (a.k.a. PECASE Award) (1996).

Dr. Pedram is a Fellow of the IEEE and the IEEE Circuits and Systems Society VP of Publications. He is also an Advisory Board Member of the ACM Interest Group on Design Automation. His current work focuses on developing computer aided design methodologies and techniques for low power design, synthesis, and physical design.